40. A. Haddow, *Acta Unio Int. Contra Cancrum* **3**, 342 (1938).
41. We thank E. Vazile in the Koch Institute Microscopy and Imaging Facility for help with SKY analysis; M. Luo in the MIT BioMicro Center for help with microarray analysis; L. Chan for assistance with the double linear fit models for immortalization kinetics; A. Regev and M. Guttman for advice and assistance with statistical analysis; and M. Dunham, M. Hemann, J. Lees, F. Solomon, and members of the Amon lab for critical reading of this manuscript. This work was supported by the Howard Hughes Medical Institute, a David Koch Research Award, a grant from the Curt W. and Kathy Marble Cancer Research Fund, and a David Koch Graduate Fellowship (V.R.P.). All microarray data are provided in final processed form in table S1 and as raw data through the Gene Expression Omnibus (www.ncbi.nlm.nih.gov/geo) under accession number GSE12501.

Supporting Online Material
www.sciencemag.org/cgi/content/full/322/5902/703/DC1
Materials and Methods
Figs. S1 to S9
Tables S1 to S4
References

5 May 2008; accepted 9 September 2008
10.1126/science.1160058

Structure and Molecular Mechanism of a Nucleobase–Cation–Symport-1 Family Transporter

Simone Weyand,[1,2,3]* Tatsuro Shimamura,[2,3,4]* Shunsuke Yajima,[2,3]*† Shun'ichi Suzuki,[5]*‡ Osman Mirza,[2]*§ Kuakarun Krusong,[2]‖ Elisabeth P. Carpenter,[1,2] Nicholas G. Rutherford,[5] Jonathan M. Hadden,[5] John O'Reilly,[5] Pikyee Ma,[5] Massoud Saidijam,[5,6] Simon G. Patching,[5] Ryan J. Hope,[5] Halina T. Norbertczak,[5] Peter C. J. Roach,[5] So Iwata,[1,2,3,4,7]¶ Peter J. F. Henderson,[5]¶ Alexander D. Cameron[1,2,3]

The nucleobase–cation–symport-1 (NCS1) transporters are essential components of salvage pathways for nucleobases and related metabolites. Here, we report the 2.85-angstrom resolution structure of the NCS1 benzyl-hydantoin transporter, Mhp1, from *Microbacterium liquefaciens.* Mhp1 contains 12 transmembrane helices, 10 of which are arranged in two inverted repeats of five helices. The structures of the outward-facing open and substrate-bound occluded conformations were solved, showing how the outward-facing cavity closes upon binding of substrate. Comparisons with the leucine transporter $LeuT_{Aa}$ and the galactose transporter vSGLT reveal that the outward- and inward-facing cavities are symmetrically arranged on opposite sides of the membrane. The reciprocal opening and closing of these cavities is synchronized by the inverted repeat helices 3 and 8, providing the structural basis of the alternating access model for membrane transport.

Many membrane transporters are classified into three major groups. One group, the primary active transporters, uses the energy released from light, redox reactions, or adenosine triphosphate (ATP) hydrolysis to translocate substrates across the membrane. Another group, the secondary active transporters, uses the free energy stored in an ion gradient for substrate transport. A third group carries out facilitated diffusion without energy input. The kinetics and thermodynamics of all types of transporters can, in principle, be explained by the alternating access model of molecular transport (*1*, *2*). According to this model, a substrate-binding site located toward the center of the protein in the membrane has alternating access to either side of the membrane as a result of reciprocal opening and closing of cavities connecting the binding site to either side of the membrane. This model is well studied and was established for various transporters with use of kinetic and biochemical methods (*3*, *4*). For the P-type adenosine triphosphatases (ATPases) and the ATP binding cassette (ABC) transporters, the mechanism has also been studied on the basis of the structures of these proteins in various conformational states (*5*, *6*). Secondary transporters are biochemically well characterized, particularly lactose permease (*7*–*9*) and other members of the major facilitator superfamily (MFS) transporters (*10*, *11*), but here the structural basis of the alternating access mechanism is less well understood.

Here, we show how structural studies of the secondary active membrane transporter, Mhp1, from *Microbacterium liquefaciens* provide insight into the mechanism of alternating access. Mhp1 mediates the uptake of indolyl methyl- and benzyl-hydantoins into *M. liquefaciens*, as part of a metabolic salvage pathway for their conversion to amino acids (*12*). Mhp1 is a member of the so-called nucleobase–cation–symport-1, NCS1, family 2.A.39 (*13*, *14*) of transport proteins, which has at least 800 known homologs in eubacteria, archaea, fungi, and plants, according to the UNIPROT (www.uniprot.org) database. Known substrates for the other NCS1 subfamily transporters include allantoin, uracil, cytosine (including the antifungals, 5-fluorocytosine and 5-fluorouracil), purines, thiamine, pyridoxal-based compounds, and nicotinamide riboside (www.membranetransport.org/) (*15*, *16*). The x-ray structure of the Mhp1 protein described in this paper reveals similarities of this cation-coupled transporter to the *Aquifex aeolicus* leucine transporter $LeuT_{Aa}$ (*17*–*19*), a member of the neurotransmitter-sodium-symporter family, NSS 2.A.22, (*13*, *16*, *20*) and to the *Vibrio parahaemolyticus* sodium-galactose symporter vSGLT (*21*), a member of the solute-sodium-symporter family, 'SSS' 2.A.21. (*13*, *16*, *22*). Despite this structural similarity, the amino acid sequence of Mhp1 exhibits only an insignificant 15% identity to $LeuT_{Aa}$ and 16% to vSGLT, as calculated by the LALIGN algorithm (www.ch.embnet.org/software/LALIGN_form.html) (*23*).

The two x-ray structures of Mhp1, in the outward-facing open conformation and in the outward-facing occluded conformation with benzyl-hydantoin, demonstrate the conformational change consequent upon the binding of substrate from the outside of the membrane. Comparison of these Mhp1 structures with those of $LeuT_{Aa}$ and vSGLT

Table 1. Refinement statistics. Resolution numbers in parentheses refer to the statistics in the highest resolution shell. $R_{factor} = \sum|F_{obs} - F_{calc}|/\sum F_{obs}$. The R_{free} is the same as the R_{factor} but for the 5% of test reflections. Ramachandran plot outliers are as defined in MolProbity (*39*).

Resolution (Å)	30–2.85 (2.92–2.85)
R_{factor} (%)	24.0 (36.3)
R_{free} (%)	28.1 (41.8)
Average *B* value (Å^2)	60.1
RMSD from ideal values	
Bonds (Å)	0.010
Angle (°)	0.982
Ramachandran plot outliers (%)	0.2

[1]Membrane Protein Laboratory, Diamond Light Source Limited, Harwell Science and Innovation Campus, Chilton, Didcot, Oxfordshire OX11 0DE, UK. [2]Division of Molecular Biosciences, Membrane Protein Crystallography Group, Imperial College, London SW7 2AZ, UK. [3]Human Receptor Crystallography Project, Exploratory Research for Advanced Technology (ERATO), Japan Science and Technology Agency, Yoshidakonoe-cho, Sakyo-ku, Kyoto 606-8501, Japan. [4]Department of Cell Biology, Graduate School of Medicine, Kyoto University, Yoshida-Konoe, Sakyo-Ku, Kyoto 606-8501, Japan. [5]Astbury Centre for Structural Molecular Biology, Institute for Membrane and Systems Biology, University of Leeds, Leeds LS2 9JT, UK. [6]School of Medicine, Hamedan University of Medical Sciences, Hamedan, Iran. [7]Systems and Structural Biology Center, RIKEN, 1-7-22 Suehiro-cho Tsurumi-ku, Yokohama 230-0045 Japan.

*These authors contributed equally to this work
†Present address: Department of Bioscience, Tokyo University of Agriculture, Sakuragaoka 1-1-1, Setagaya-ku, Tokyo 156-8502, Japan.
‡Present address: Aminosciences Laboratories, Ajinomoto Company Incorporated, 1-1 Suzuki-cho, Kawasaki-ku, Kawasaki-shi, Kanagawa 210-8681, Japan.
§Present address: Department of Medicinal Chemistry, Faculty of Pharmaceutical Sciences, University of Copenhagen, Universitetsparken 2, DK-2100, Denmark.
‖Present address: Department of Biochemistry, Faculty of Science, Chulalongkorn University, Phyathai Road, Patumwan, Bangkok 10330, Thailand.
¶To whom correspondence should be addressed. E-mail: s.iwata@imperial.ac.uk (S.I.); p.j.f.henderson@leeds.ac.uk (P.J.F.H.)

suggests a possible further conformational change, which allows the release of the substrate into the inside of the membrane. The inward- and outward-facing cavities of the transporters are symmetrically arranged on the opposite sides of the membrane by using two inverted repeated segments related by an internal pseudo-twofold axis parallel to the membrane. This comparative study suggests how the reciprocal opening and closing of inward-facing and outward-facing cavities could be synchronized by helices 3 and 8 that connect the two cavities on the opposite sides of the membrane.

Structure determination. For details, see (*24*). The structure of Mhp1 without substrate was solved by using multiple isomorphous replacement in combination with twofold cross-crystal averaging (*25*). The model was refined against data extending to a resolution of 2.85 Å with an R_{factor} of 24.0% and a corresponding R_{free} of 28.1% (Table1, table S1 and fig. S1) (*26*). The structure of the complex of Mhp1 with benzyl-hydantoin was solved from crystals grown in the presence of the substrate. Despite the limited resolution (4 Å), difference maps showed that the substrate is present in the binding site and that there is a structural rearrangement of residues 355-370. To avoid over-refinement, we only remodeled this region, followed by minimization with strict harmonic restraint (*24*). This partially remodeled structure gave an R_{factor} of 34.2% and a corresponding R_{free} of 39.2% (*24*).

Transporter architecture. The structure is composed of 12 membrane-spanning helices as was predicted (Fig. 1A) (*12*), although previous assignment of transmembrane helices (TMs) based on homologous yeast NCS-1 transporters needed a slight revision (fig. S2) (*15*). The 12 transmembrane helices (TMs) are arranged in two repeating units (TMs 1 to 5, residues 20 to 190, and TMs 6 to 10, residues 209 to 388) connected by an 18-residue loop and followed by an additional two transmembrane helices (Fig. 1, A and B). The similarity of the two repeating units is such that 65 out of a possible 170 Cα pairs can be superimposed with a root mean square deviation (RMSD) of 2.5 Å (*24*), despite the absence of significant sequence homology between the two units. The two units show an opposite topology with respect to the membrane and are related to each other by a rotation of 168° around an axis in the center of the membrane and parallel to its plane. An inverted topology repeat is commonly observed for many membrane transporters and channels (*17*, *21*, *27*–*31*). The two repeat units are completely intertwined, giving a central four-helix bundle consisting of the two broken TMs, 1 and 6, associated with TMs 2 and 7 (Fig. 1). This bundle is coated, on the side of TMs 1 and 6, by a layer formed by the other six helices; TMs 3 and 8, facing directly toward TMs 1 and 6, form a long antiparallel unit threading through two V-shaped structures formed by TMs 4 and 5 and TMs 9 and 10, respectively (Fig. 1A). The substrate- and cation-binding sites and the outward-facing cavity connecting these sites to the outsides of the

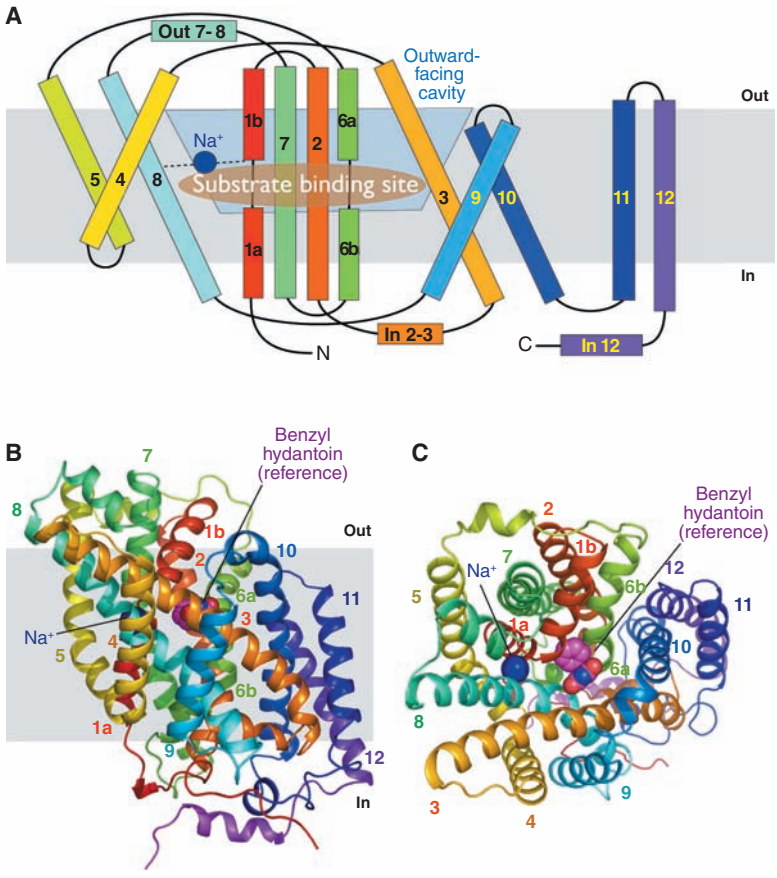

Fig. 1. Structure of Mhp1 from *M. liquefaciens.* (**A**) Mhp1 topology. The positions of the substrate- and the cation-binding sites are depicted as a brown ellipsoid and a blue circle, respectively. The membrane is shown in gray, and the outward-facing cavity observed in the structure is highlighted in light blue. The horizontal helices on the inside and outside of membrane are indicated as In and Out. TMs 3 and 8 pack onto each other in three-dimensional space. (**B**) The Mhp1 structure viewed in the plane of the membrane. The image is based on the high-resolution structure of the Mhp1 without benzyl-hydantoin. The position of the substrate in the Mhp1—benzyl-hydantoin complex structure is shown as a reference. A sodium ion is also shown and labeled. (**C**) View from the outside of the membrane.

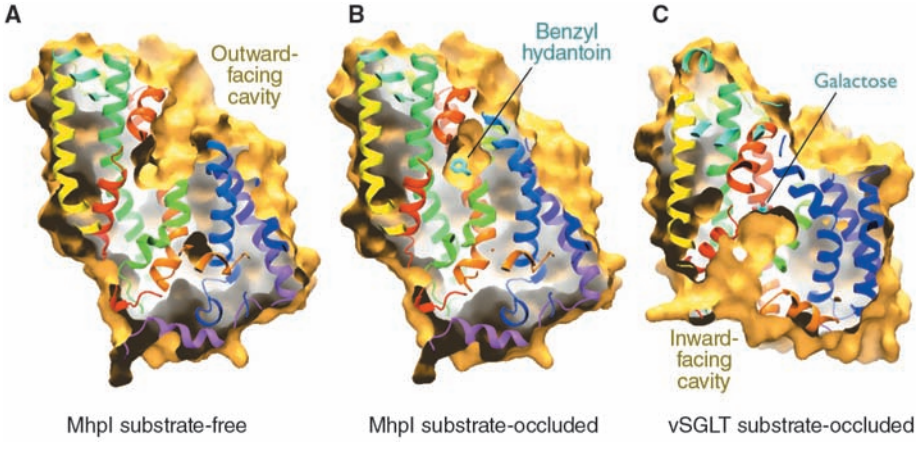

Fig. 2. Outward- and inward-facing cavities. (**A**) A slice through the surface of the Mhp1 substrate-free structure, viewed parallel to the membrane, showing the outward-facing cavity. The Connolly surface of Mph1 is shown in yellow (calculated with a probe radius of 2 Å). The ribbon representation of Mhp1 is colored as in Fig. 1. (**B**) As for (A) but for the Mhp1 substrate-occluded structure. Bound benzyl-hydantoin is shown in cyan. Note that the outward-facing cavity shown in (A) is blocked and the substrate is occluded from the outside of the membrane. (**C**) As for (A) but for the vSGLT substrate-occluded structure (PDB accession code 3DH4), showing the inward-facing cavity. Bound galactose is shown in cyan and red.

membrane are all located in the space between the central four-helix bundle and the outer helix layer (Figs. 1 and 2).

The amino acid sequence for TMs 11 and 12 and the C-terminal extension is poorly conserved among the NCS1 family (fig. S2), and the structural role of this region is unclear.

Although from the respective sequences it was not obvious, the fold of the core 10 helices of Mhp1 (TMs 1–10) is reminiscent of those of $LeuT_{Aa}$ (TMs 1-10) (*17*) and the recently solved structure of vSGLT (TMs 2-11) (*21*) (fig. S3). Overall, 249 out of a possible 460 Cα pairs between $LeuT_{Aa}$ and Mhp1 can be superimposed with a RMSD of 2.4 Å (*24*). Using the same algorithm to superpose Mhp1 and vSGLT, 172 Cα atom pairs have an rms deviation of 2.2 Å (fig. S4).

Substrate binding and conformational changes. In the electron density maps of the Mhp1 crystals with benzyl-hydantoin (Fig. 3, A and B), a V-shaped density was clearly observed at a position almost identical to that of the leucine in the $LeuT_{Aa}$ structure and close to that of the galactose in vSGLT (fig. S5). This site is located at the breaks in the discontinuous TMs 1 and 6 and facing TMs 3 and 8 (Fig. 1). It is located at the foot of the outward-facing cavity, which is composed of the neighboring surfaces of TMs 1, 3, 6, 8, and 10 and allows access of the substrate to the binding site (Figs. 1 and 2A). The structure of L-5-benzyl-hydantoin taken from the Cambridge Structural Database (accession code IWEYAK) was consistent with the shape of this density and the molecule was placed between Trp^{117} (TM3) and Trp^{220} (TM6) without requiring any modifications of torsion angles (Fig. 3, A and B).

In the current model, the hydantoin moiety forms a *pi*-stacking interaction with the indole-ring of Trp^{117} and is within hydrogen bonding distance of Asn^{318} and Gln^{121} (Fig. 3A). Trp^{117} and Asn^{318} are conserved amongst all the transporters in the family and Gln^{121} only varies in the uridine transporter, FUI 1 (fig. S2). Another conserved residue, Asn^{314}, is within hydrogen bonding distance of Asn^{318} such that it may hold the asparagine side chain in position to interact with the substrate. The benzyl group of the substrate is situated next to Trp^{220} and Gln^{42}. The side chain of Trp^{220} moves into the binding site with respect to its position in the substrate-free structure and forms a pi-stacking interaction with the benzyl moiety.

This binding mode is consistent with the observation that Mhp1 has a higher affinity for 5-indolyl-methyl-hydantoin than for benzyl-hydantoin (*12*), because the indole group in the hydantoin would form an even more extensive packing interaction with Trp^{220} and, in addition, the side chain of Gln^{42} could form a hydrogen bond with the nitrogen atom of the indole rings. This residue could play a role in the substrate specificity of the NCS1 transporters as suggested by sequence analysis (*15*).

The observed residues in the substrate-binding site are consistent with the results of mutational studies on a NCS1 family member, Fcy2, that transports cytosine into *Saccharomyces cerevisae* (*32*–*35*). Although Fcy2 is a distantly related homolog of Mhp1, the residues involved in the substrate and cation binding can be aligned with Mhp1 unambiguously (fig. S2). Three of the genetically selected Fcy2 mutants, which show an altered Michaelis constant K_m of substrate uptake, were substitutions in the segment 371 I-A-N-N-I-P-N 377 (*36*) of Fcy2, which corresponds to the residues 311 to 318 of Mhp1 (*32*–*34*). Site-directed mutagenesis studies on these residues emphasized the role in the substrate binding of Asn^{374} and Asn^{377}, which are equivalent to Asn^{314} and Asn^{318} of Mhp1, respectively (*35*).

In the benzyl-hydantoin complex structure, some conformational differences from the substrate-free Mhp1 structure are evident (Fig. 3, C and D). The N-terminal part of TM10 (residues 355 to 370) moves into the outward-facing cavity. This occludes the substrate-binding site from the outside space of the membrane (Figs. 2B and 3C).

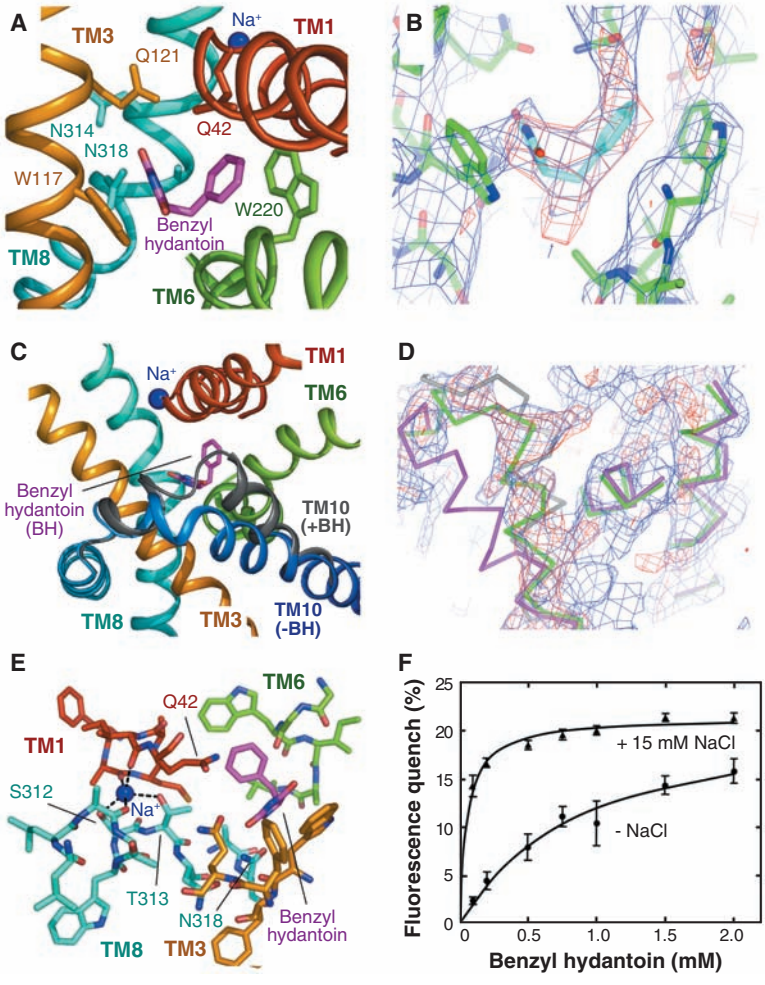

Fig. 3. Substrate- and cation-binding sites. (**A**) Substrate-binding site. The helices and key interacting residues (*36*) of the site are shown. The benzyl-hydantoin and the nearby sodium are shown in magenta and blue, respectively. (**B**) Electron density associated with benzyl-hydantoin. The $2F_o$–F_c map (blue) has been contoured at 0.6σ and the F_o–F_c map (red) at 3σ. (**C**) The conformational change upon the substrate binding. Transmembrane helix (TM) 10 and the loop between TMs 9 and 10 show a conformational change that occludes the bound substrate from the outside of the membrane. The trace of this region, shown in gray, is superimposed on the substrate-free structure. Benzyl-hydantoin is abbreviated as BH in the figure. (**D**) Electron density and model for TM10. The $2F_o$–F_c map (blue) has been contoured at 0.6σ and the F_o–F_c map (red) at 2σ. The trace for the benzyl-hydantoin free structure is shown in magenta and that for the benzyl-hydantoin complex is depicted in green. The gray trace is for the vSGLT structure (PDB accession code 3DH4) superimposed onto Mhp1. The maps in (B) and (D) were calculated on the basis of the molecular replacement solution by using the substrate-free structure with residues 355 to 370 omitted so is not biased by these residues [see (*24*) for details]. (**E**) Helices and key residues surrounding the cation- and substrate-binding sites. (**F**) Tryptophan-fluorescence-quenching by benzyl-hydantoin. The Mhp1 solution was titrated by benzyl-hydantoin and the decrease in the tryptophan fluorescence at 348 nm was monitored. The measurements were performed with (triangles) and without (circles) 15 mM NaCl in the solution. For details, see (*24*). Error bars indicate the standard error of the mean (n = 3).

This movement seems to be triggered by a repositioning of Trp^{220} located on TM6, which is adjacent to TM10.

We, therefore, have two conformations of the protein. We refer to the substrate-free structure as outward-facing open and to the substrate bound structure as outward-facing occluded.

Occluding the substrate-binding site from the outside of the membrane is essential to prevent the leakage of any molecules across the membrane. In $LeuT_{Aa}$, it was proposed that this should be achieved by the interactions between TMs 1 and 8 and TMs 6 and 3 (*17*). The binding site is occluded by the side chains of selected residues that pack over the substrate in $LeuT_{Aa}$. The occluding mechanism of the outward-facing cavity for Mhp1, therefore, seems to be different from that for $LeuT_{Aa}$. It is noteworthy that in the closed vSGLT outward-facing cavity (*21*), TM11 (equivalent to TM10 of Mhp1) adopts a conformation similar to TM10 in the occluded form of Mhp1 (Fig. 3D).

Cation-binding site. The electron density map at 2.85 Å resolution indicates a possible cation-binding site at the C-terminal end of TM1a interacting with TM8. The site includes the carbonyl-oxygen-atoms of Ala 38, and Ile 41 of TM1 and the carbonyl-oxygen-atom of Ala 309, and the hydroxyl-oxygen-atoms of the side chains of Ser 312 and Thr 313, respectively (Fig. 3E and fig. S6). Presumably the dipole moment at the C terminus of TM1a contributes to the binding as seen for other transporters (*17*, *21*, *27*, *28*, *30*). Currently, a sodium ion is modeled at this position such that the substrate atoms form a square pyramidal arrangement with the bond distances between 2.2 and 2.7 Å, which is too short for a water molecule. An equivalent site was observed and assigned as a sodium binding site in the structures of $LeuT_{Aa}$ and vSGLT (fig. S6). The connection between the cation-binding site and the substrate-binding site could be made by residue Asn^{318} on TM8 and Gln^{42} on TM1. A requirement for cation-binding to form a proper substrate-binding site provides a basis for the coupling of the cation and substrate translocation.

To confirm the sodium dependency of Mhp1, which was not evident in whole cell uptake experiments (*12*), the binding of benzyl-hydantoin and/or sodium was measured using fluorescence quenching (Fig. 3F) (*37*). The results clearly show that the affinity of benzyl-hydantoin to the protein [apparent dissociation constant (K_d) of 0.88 ± 0.27 mM] is raised over 10-fold in the presence of 15 mM sodium (apparent K_d 0.054 ± 0.007 mM). We have also observed that the benzyl-hydantoin increases the affinity of sodium to Mhp1; in the absence of benzyl-hydantoin, the apparent K_d for sodium is 1.15 ± 0.28 mM, and in the presence of 2 mM benzyl-hydantoin, the value is 0.15 ± 0.04 mM. These results indicate that the binding of sodium and benzyl-hydantoin are tightly coupled in Mhp1.

Some of the NCS1 family transporters from yeasts and bacteria, including Mhp1, were thought to be proton- rather than sodium-dependent (*12*, *15*, *16*). Sodium dependence in whole cell transport assays may be obscured by the presence of a separate compensating sodium transport system in the membrane. In the case of Mhp1 the sensitivity of assays is reduced by the low solubility and the lipophilic nature of the substrate, preventing the testing of sodium dependence in proteoliposomes. It is also possible that Mhp1 and other NCS-1 transporters have a flexible cation selectivity, like the MelB sugar-cation symporter (*38*).

Possible transport mechanism. The two structures of Mhp1 reveal the conformational change of the transporter upon the binding of substrate from the outside of the membrane. The structure of vSGLT provides further insight into the transport process because it is in an inward-facing conformation closed with the substrate in its binding site (Figs. 2C and 4). We refer to this as an inward-facing, occluded conformation according to the assignment in (*21*). There, the cavity connecting the substrate-binding site to the inside of the membrane is observed although the site is still occluded (Fig. 2C and figs. S7 and S8). In this vSGLT structure the outward-facing cavity, as also observed in $LeuT_{Aa}$ and substrate-bound Mhp1, is completely closed (Fig. 2C). The observed inward-facing cavity in vSGLT is made of the neighboring surfaces of TMs 1, 3, 5, 6, and 8 (Fig. 2C and figs. S7 and S8), which are symmetrically related to the outward-facing cavity observed in Mhp1 on the opposite side of the membrane. Thus, these structures are related by an approximate two-fold axis that is parallel to the membrane (fig. S7). In Fig. 4, we compare the conformations of the core 10 helices (TMs 1 to 10) of outward-facing Mhp1 and inward-facing vSGLT. These structures suggest a reciprocating oscillation between symmetrical states opening alternately to each side of the membrane.

In the following, we propose a possible mechanism of molecular transport across the membrane by Mhp1 based on the x-ray structures (Fig. 4).

1) Change of the outward-facing open state to the outward-facing occluded state: In Mhp1, the outward-facing cavity is formed by TMs 1, 3, 6, 8, and 10 (Figs. 1C and 2A). Upon the binding of the substrate, TM10 moves toward the cavity closing access to the outside space of the membrane (Figs. 2B and 4).

2) Change of the outward-facing occluded state to the inward-facing occluded state: In vSGLT, the inward-facing cavity is formed by TMs 1, 3, 5, 6, and 8 (Mhp numbering, figs. S7 and S8). In the structure, the substrate-binding site is occluded from the inside of the membrane. In the outward-facing conformation of Mhp1 (and $LeuT_{Aa}$), the inward-facing cavity observed in vSGLT is occupied by TM8 (and partly by TM6). On the other hand, in the inward-facing conformation of vSGLT, the outward-facing cavity is occupied by TM3 (and partly TM6). It seems that the alternation of the outward- and inward-facing conformations is effected by the movement of the helix bundle of TMs 3 and 8. It is also possible that TMs 1 and 6 undergo a coordinated shift with TMs 3 and 8, as proposed by Gouaux and co-workers (*17*). Because of the substantial difference in the substrate binding sites of Mhp1 and vSGLT, it is difficult to estimate the extent of the movement of TMs 1 and 6; thus, in Fig. 4 only TMs 3 and 8 are shown for simplicity.

3) Change of the inward-facing occluded state to the inward-facing open state: This transition is required to release the substrates to the inside, but no structures are available to define this change. For vSGLT, it is proposed that the movement of Tyr^{263} is enough to open up the cavity (*21*). For Mhp1, in addition, the opening up of TMs 4 and 5 might be necessary. The connection between TMs 4 and 5 is disordered and is not modeled in vSGLT. If this connection has a similar conformation to the one in Mhp1, it would block the cavity.

The site of the cation uptake and release is also controlled by the conformational changes, because the ion-binding site is located between TMs 1 and 8 (Fig. 4D). The cation-binding sites of Mhp1 and $LeuT_{Aa}$ are very similar (fig. S6) and are a part of the surface of the outward-facing cavity, whereas the one for vSGLT is very different and is a part of the inward-facing cavity, occurring as a consequence of the conformational change of TMs 3 and 8. This, together with the strong coupling of substrate and cation binding, should form the basis of substrate-cation symport. The coordinated and reciprocating conformational

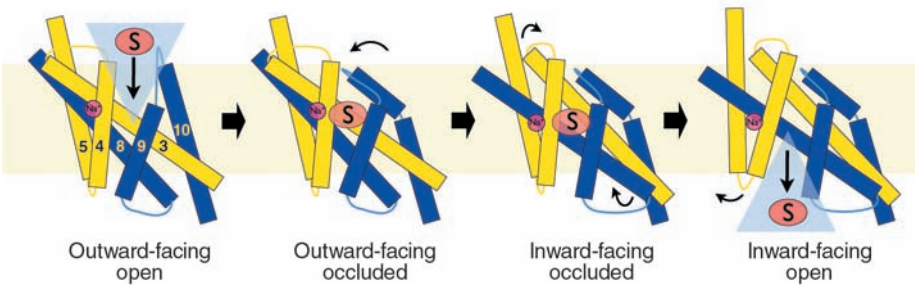

Fig. 4. Proposed substrate translocation mechanism by Mhp1. Schematic diagram showing four different conformational states: outward-facing open, outward-facing occluded, inward-facing occluded, and inward-facing open. Substrate- and sodium-binding sites are labeled as S and Na^+, respectively.

changes observed on both sides of the membrane provide a structural basis for the widely held view of an alternating access model deduced from kinetics data.

References and Notes

1. O. Jardetzky, *Nature* **211**, 969 (1966).
2. C. Tanford, *Proc. Natl. Acad. Sci. U.S.A.* **80**, 3701 (1983).
3. H. R. Kaback *et al.*, *Proc. Natl. Acad. Sci. U.S.A.* **104**, 491 (2007).
4. D. D. F. Loo, B. A. Hirayama, M. H. Karakossian, A. K. Meinild, E. M. Wright, *J. Gen. Physiol.* **128**, 701 (2006).
5. C. Toyoshima, *Arch. Biochem. Biophys.* **476**, 3 (2008).
6. K. Hollenstein, R. J. Dawson, K. P. Locher, *Curr. Opin. Struct. Biol.* **17**, 412 (2007).
7. O. Mirza, L. Guan, G. Verner, S. Iwata, H. R. Kaback, *EMBO J.* **25**, 1177 (2006).
8. J. Abramson *et al.*, *Science* **301**, 610 (2003).
9. L. Guan, O. Mirza, G. Verner, S. Iwata, H. R. Kaback, *Proc. Natl. Acad. Sci. U.S.A.* **104**, 15294 (2007).
10. Y. Huang, M. J. Lemieux, J. Song, M. Auer, D. N. Wang, *Science* **301**, 616 (2003).
11. Y. Yin, X. He, P. Szewczyk, T. Nguyen, G. Chang, *Science* **312**, 741 (2006).
12. S. Suzuki, P. J. Henderson, *J. Bacteriol.* **188**, 3329 (2006).
13. M. H. Saier Jr., *Adv. Microb. Physiol.* **40**, 81 (1998).
14. M. H. Saier Jr., C. V. Tran, R. D. Barabote, *Nucleic Acids Res.* **34**, D181 (2006).
15. A. Pantazopoulou, G. Diallinas, *FEMS Microbiol. Rev.* **31**, 657 (2007).
16. Q. Ren, K. Chen, I. T. Paulsen, *Nucleic Acids Res.* **35**, D274 (2007).
17. A. Yamashita, S. K. Singh, T. Kawate, Y. Jin, E. Gouaux, *Nature* **437**, 215 (2005).
18. S. K. Singh, A. Yamashita, E. Gouaux, *Nature* **448**, 952 (2007).
19. Z. Zhou *et al.*, *Science* **317**, 1390 (2007); published online 9 August 2007 (10.1126/science.1147614).
20. L. Shi, M. Quick, Y. Zhao, H. Weinstein, J. A. Javitch, *Mol. Cell* **30**, 667 (2008).
21. S. Faham *et al.*, *Science* **321**, 810 (2008); published online 3 July 2008 (10.1126/science.1160406).
22. E. Turk *et al.*, *J. Biol. Chem.* **275**, 25711 (2000).
23. X. Huang, W. Miller, *Adv. Appl. Math.* **12**, 337 (1991).
24. Materials and methods are available as supporting material on *Science* Online.
25. K. Cowtan, *Joint CCP4 and ESF-EACBM Newsletter on Protein Crystallography* **31**, 34 (1994).
26. P. D. Adams *et al.*, *Acta Crystallogr. D* **58**, 1948 (2002).
27. C. Hunte *et al.*, *Nature* **435**, 1197 (2005).
28. D. Yernool, O. Boudker, Y. Jin, E. Gouaux, *Nature* **431**, 811 (2004).
29. D. Fu *et al.*, *Science* **290**, 481 (2000).
30. R. Dutzler, E. B. Campbell, M. Cadene, B. T. Chait, R. MacKinnon, *Nature* **415**, 287 (2002).
31. J. U. Bowie, *Nat. Struct. Mol. Biol.* **13**, 94 (2006).
32. M. R. Chevallier, R. Jund, F. Lacroute, *J. Bacteriol.* **122**, 629 (1975).
33. J. C. Bloch, H. Sychrova, J. L. Souciet, R. Jund, M. R. Chevallier, *Mol. Microbiol.* **6**, 2989 (1992).
34. D. Brèthes *et al.*, *Eur. J. Biochem.* **204**, 699 (1992).
35. T. Ferreira, D. Brèthes, B. Pinson, C. Napias, J. Chevallier, *J. Biol. Chem.* **272**, 9697 (1997).
36. Single-letter abbreviations for the amino acid residues are as follows: A, Ala; I, Ile; N, Asn; P, Pro; Q, Gln; S, Ser; T, Thr; and W, Trp.
37. P. J. Henderson, G. E. Martin, T. P. McDonald, A. Steel, A. R. Walmsley, *Antonie Leeuwenhoek* **65**, 349 (1994).
38. T. H. Wilson, P. Z. Ding, *Biochim. Biophys. Acta* **1505**, 121 (2001).
39. S. C. Lovell, *Proteins* **50**, 437 (2003).

40. This research was funded primarily by the Biotechnology and Biological Sciences Research Council (grant nos. B17935 and BB/C51725), with important contributions from Ajinomoto Incorporated, the European Membrane Protein consortium (grant no. LSHG-CT-2004-504601), the Membrane Protein Structure Initiative (grant no. BBS/B/14418), and the Wellcome Trust (grant no. 062164/Z/00/Z). We wish to thank the Membrane Protein Laboratory (MPL) at the Diamond Light Source Limited for use of the MPL facilities. J. Abramson kindly provided us with the coordinates of vSGLT before their release from the Protein Data Bank (PDB). We are also grateful to S. Phillips, S. Baldwin, P. Gilmartin, S. Radford, D. Drew, M. Jormakka, K. Watanabe, and M. Iwata for support or advice. The Japan Society for the Promotion of Science provided personal funding to S.Y. and the Leverhulme Trust to P.J.F.H. S.W. was a recipient of a European Molecular Biology Organization long-term fellowship. The coordinates and the structure factors for Mhp1 without substrate and the hydantoin complex have been deposited in the PDB (entries 2JLN and 2JLO, respectively).

Supporting Online Material

www.sciencemag.org/cgi/content/full/1164440/DC1
Materials and Methods
Table S1
Figs. S1 to S8
References

8 August 2008; accepted 26 September 2008
Published online 16 October 2008;
10.1126/science.1164440
Include this information when citing paper.

REPORTS

Magnetism on the Angrite Parent Body and the Early Differentiation of Planetesimals

Benjamin P. Weiss,[1]* James S. Berdahl,[1] Linda Elkins-Tanton,[1] Sabine Stanley,[2] Eduardo A. Lima,[1] Laurent Carporzen[1]

Angrites are among the oldest known pristine basaltic meteorites and record the earliest stages of planet formation and differentiation. Our paleomagnetic analysis of three angrites found that they record a past magnetic field of ~10 microteslas on the angrite parent body extending from 4564 to at least 4558 million years ago. Because the angrite paleomagnetic record extends beyond the expected lifetime of the early circumstellar disk, these paleofields were probably generated internally on the angrite parent body, possibly by an early dynamo in a rapidly formed metallic core.

Basaltic achondrites are thought to be igneous samples of the first differentiated planetary bodies. Several classes of these meteorites have crystallization ages within just ~3 million years (My) of the formation of the solar system and contain geochemical signatures of metal and silicate fractionation. Remanent magnetization has been detected in meteorites from five basaltic achondrite groups, indicating the presence of past magnetic fields on these bodies (*1*). However, these meteorites, as well as nearly all basaltic achondrite groups, were subjected to brecciation, shock, and metamorphic events tens to hundreds of millions of years after their formation that modified and, in many cases, reset their magnetization. Because magnetic fields can be generated by large impacts (*2*), the fields recorded on these bodies also may not have been generated internally.

An exception is the angrites, a group of twelve basaltic achondrites from an as yet unidentified parent body. Angrites have Pb/Pb and Hf/W ages of 4564 to 4558 million years ago (Ma) (*3*–*5*) that are within error of their (U-Th)/He ages for all but two meteorites (*6*). They entirely lack shock, post-cooling brecciation, and parent-body weathering textures (*7*–*12*), which makes them among the best preserved materials known from the early solar system. Angrites may therefore record two fundamental field-generating mechanisms postulated to exist in the early solar system: stellar and circumstellar disk fields external to the angrite parent body (APB) and an internal core dynamo on the APB.

Here we present a paleomagnetic investigation of 3 of the 12 known angrites: Angra dos Reis, D'Orbigny, and Asuka (A) -881371. We found that the angrites Northwest Africa (NWA) 2999 and NWA 4801 have been substantially remagnetized by collectors' hand magnets (as indicated by communication with previous owners of the samples and moments near saturation), whereas NWA 4931 has been heavily weathered

[1]Department of Earth, Atmospheric, and Planetary Sciences, Massachusetts Institute of Technology, 54-814, 77 Massachusetts Avenue, Cambridge, MA 02139, USA. [2]Department of Physics, University of Toronto, 60 St. George Street, Toronto, ON M5S 1A7, Canada.

*To whom correspondence should be addressed. E-mail: bpweiss@mit.edu